Apatite Chemistry And Its Application To The Hydrothermal Evolution Of The Se-Chahun Magnetite-Apatite Deposit

Zahra Bonyadia, Behzad Mehrabi, Garry J. Davidson, Sebastien Meffre and Fereydoun Ghazban

a Geology Department, Tarbiat Moallem University, Tehran, Iran, z_bonyadi@tmu.ac.ir, 09124109039

Abstract

Se-Chahun Magnetite-apatite deposit is located in the Bafq district, Central Iran. The deposit comprises two major orebodies, anomaly X and XI. The anomalies are located in: 31° , 52′, 30″ N ; 55° , 42′, 07″ E and 31° , 54′, 20″ N ; 55° , 43′, 57″ E respectively. The deposit contains an overall resource of 117.6 Mt of high-grade Fe ore. The Se-Chahun deposit is considered to be an example of a Kiruna-type deposit. The host rocks in both anomalies have undergone widespread Na metasomatism (chessboard albite), followed by Na-Ca metasomatism (amphibole-albite-magnetite-calcite-epidote-quartz-titanite-allanite), mineralization (magnetite-apatite), K-metasomatism (K-feldspar and less amounts of biotite), brecciation and carbonate veining. Sulfide minerals are rarely present in the ore or wallrocks. Where present, they are associated with a paragenetically late calcite-quartz-chlorite-(hematite) assemblage, and are dominated by pyrite with subsidiary chalcopyrite. The earliest mineralization products consisted of semi-massive magnetite intergrown with coarse apatite. High resolution back scattered electron images (BSE) of the coarse apatite grains show some heterogeneous zonation patterns in single apatite grains. The dark and bright zones in Se-Chahun apatite are mainly patchy and irregular. Electron microprobe analysis (EMPA), and laser ablation-inductively coupled plasma-mass spectrometry (LA–ICPMS) techniques were employed to determine the difference between the chemical composition of the bright and dark areas in the apatite. Following the development of magnetite-apatite assemblage, prior to brecciation, K-Cl rich fluids changed most primary apatite (SEM-bright) to SEM-dark apatite by leaching LREE+Y, Na, Cl, Si, S and As and adding Ca and P. Monazite inclusions were produced at this stage in the dark apatite areas. Monazite also formed after apatite brecciation. It is concluded that LREE+Y, P, Ti and Al had restricted mobility in the hydrothermal evolution of the deposit. Other elements such as S, Fe and As had greater mobility in the system. Apatite and magnetite growth appears to have been contemporaneous with the sodic-calcic alteration, but immediately prior to brecciation. This process provides a window into hydrothermal evolution during and after mineralization, that lead immediately to brecciation, presumably driven by larger-scale volatile release.

Keywords: *apatite, Se-Chahun, dark, bright, hydrothermal, metasomatism*.

Kiruna-type and Fe oxide–Cu(-Au) deposits are considered by [1] to be end members of a continuum of mineralized systems that typically developed in post-Archean tectonic regimes characterized by igneous activity. Se-Chahun and other Fe-oxide-apatite deposits in the Bafq district have various mineralogical and geochemical characteristics that are typical of the Kiruna-type magnetite-apatite end member.

The mineralization is hosted by metasomatized (altered) rhyolitic tuffs and intercalated shallow-water sediments, sandstone, dolomitic limestone and shale, which represent the middle sequence of the Saghand Formation [2]. The host rocks in both anomalies were

strongly affected by both early sodic (chessboard albite) and pervasive sodic-calcic alteration (amphibole-albite-magnetite–apatite-calcite-epidote-quartz-titanite-allanite).

Sodic–calcic alteration is accompanied by magnetite ± apatite formation (in all orebodies) and follows by potassic alteration (in anomaly XI), chloritization, carbonate veining, and hydrolytic alteration.

There are two different types of apatite in Se-Chahun iron deposit. The first type consists of small apatite inclusions within the magnetite grains, present in all orebodies of the deposit. Due to the small size of the apatite of this group (less that 40 μ), their chemical analysis was unreliable. The second group is represented by coarse euhedral up to 4 cm long crystals. This group is only observed in anomaly X.

High resolution back scattered images of the latter show some heterogeneous zonation patterns in single apatite grains (Figs. 8A and 8B). [3] reported the same feature in apatite from Kirrunavaara magnetite-apatite deposit. The dark and bright zones in apatite are mainly patchy and irregular, but it seems that the development of the dark areas in apatite shows a preferred orientation (i.e. parallel to crystallographic c-axis). The patterns continue through brecciated zones as well, and the cracks and fractures do not have affected on the patterns. Thus it is concluded that the brecciation has occurred afterward (Figs. 8A and 8B).

In general, numerous fluid inclusions are scattered in the dark areas. However some dark areas do not include inclusions (Fig. 8B). The frequency of fluid and solid inclusions is much less in bright areas of apatite.

Electron microprobe analysis (EMPA), and laser ablation-inductively coupled plasma-mass spectrometry (LA–ICPMS) techniques were employed to determine the difference between the chemical composition of the bright and dark areas in the apatite (Table 1, Fig. 2). The difference between the areas is mainly due to different concentrations of REE and some trace elements, such as Si, Na, Cl and F. Rare earth elements have large atomic weights and produce more back-scattered electrons, hence, apatite with an elevated REE concentration shows a brighter image, while dark domains are depleted in REE. In all samples, Na2O, SiO2, Cl, FeO, SO3 and LREE contents in bright areas are significantly higher than those of dark areas (Table 1). In some samples, the concentration of some elements such as S and La are less than detection limit in dark areas.

Monazite inclusions were produced due to the leaching of primary (bright) apatite and producing the dark apatite areas. Monazite formed in the dark apatite zones and in the matrix of the apatite breccias produced as a result of brecciation.

It is concluded that LREE+Y, P, Ti and Al had restricted mobility in the hydrothermal evolution of the deposit. Other elements such as S, Fe and As had greater mobility in the system. Apatite and magnetite growth appears to have been contemporaneous with the sodic-calcic alteration, but immediately prior to brecciation.

It appears that apatite metasomatism took place when Na-rich and/or Ca bearing fluids responsible for the Na-metasomatism and Na-Ca metasomatism were not active, as they prevent the nucleation of monazite, by stabilizing apatite structure. Apatite metasomatism occured as a result of K-rich fluids circulation in the ore [4] and [5]. The fluids are also responsible for the K- metasomatism in the host rocks.

References

[1] Hitzman, M.W., 2000. Iron oxide-Cu-Au deposits: what, where, when, and why. Pp. 9-25 in: Hydrothermal Iron Oxide Copper-gold & Related Deposits: A Global Perspective (T.M. Porter, editor), 2, PGC Publishing, Adelaide, Australia.

[2] Samani, B., 1993. Saghand formation, a riftogenic unit of upper Precambrian in central Iran. Geosciences: Scientific Quarterly Journal of the Geological Survey of Iran, 2, 32-45 (in Farsi with English abstract).

[3] Harlov, D.E., Andersson, U.B., Fo¨rster, H.J., Nystro¨m, J.O., Dulski, P. and Broman, C., 2002. Apatite monazite relations in the Kiirunavaara magnetite-apatite ore, northern Sweden. Chemical Geology, 191, 47-72.

[4] Giere´, R., 1989. Hydrothermal mobility of Ti, Zr and REE: examples from the Bergell and Adamello contact aureoles (Italy). Terra Nova, 2, 60-67.

[5] Harlov , D.E., Wirth, R. and Förster, H.J., 2005. An experimental study of dissolution-reprecipitation in fluorapatite: fluid infiltration and the formation of monazite. Contri to Miner. and Petro., 150, 268-286.

Table 1: Trace element concentration (wt %) in bright and dark parts of the apatites of anomaly X, measured by EPMA technique.

sample	X.205-2-bright	X.205-5-bright	To22-1-bright	To22-10-bright	X.205-2-dark	X.205-5-dark	X.205-25-dark	To22-11-dark	To22-a-1-dark
P_2O_5	40.15	40.51	40.14	39.88	40.70	41.16	40.78	40.53	40.78
CaO	51.58	52.19	51.56	51.21	53.44	53.24	53.32	53.08	53.09
Na_2O	0.24	0.16	0.19	0.33	<0.07	<0.07	<0.07	<0.07	<0.07
SiO_3	0.20	0.11	0.16	0.30	0.16	0.10	0.15	0.13	0.17
FeO	0.12	0.05	0.36	0.09	<0.04	<0.04	<0.04	0.02	<0.04
SO_3	0.08	0.05	0.05	0.11	<0.03	<0.03	<0.03	<0.03	<0.03
As_2O_5	<0.04	0.06	0.05	<0.04	<0.04	<0.04	<0.04	<0.04	<0.04
Y_2O_3	0.18	0.13	0.16	0.23	<0.07	0.13	0.08	0.14	0.09
La_2O_3	0.30	0.22	0.25	0.44	0.10	<0.09	<0.09	<0.09	<0.09
Ce_2O_3	0.76	0.44	0.57	1.00	0.19	<0.1	0.21	0.12	0.25
Nd_2O_3	0.32	0.23	0.25	0.39	<0.14	<0.14	<0.14	<0.14	0.16
EuO	<0.07	<0.07	<0.07	<0.07	<0.07	<0.07	<0.07	<0.07	<0.07
Cl	1.11	0.74	1.12	1.02	0.25	0.44	0.27	0.52	0.38
F	2.84	2.82	2.76	2.76	3.29	2.97	3.16	3.07	2.94

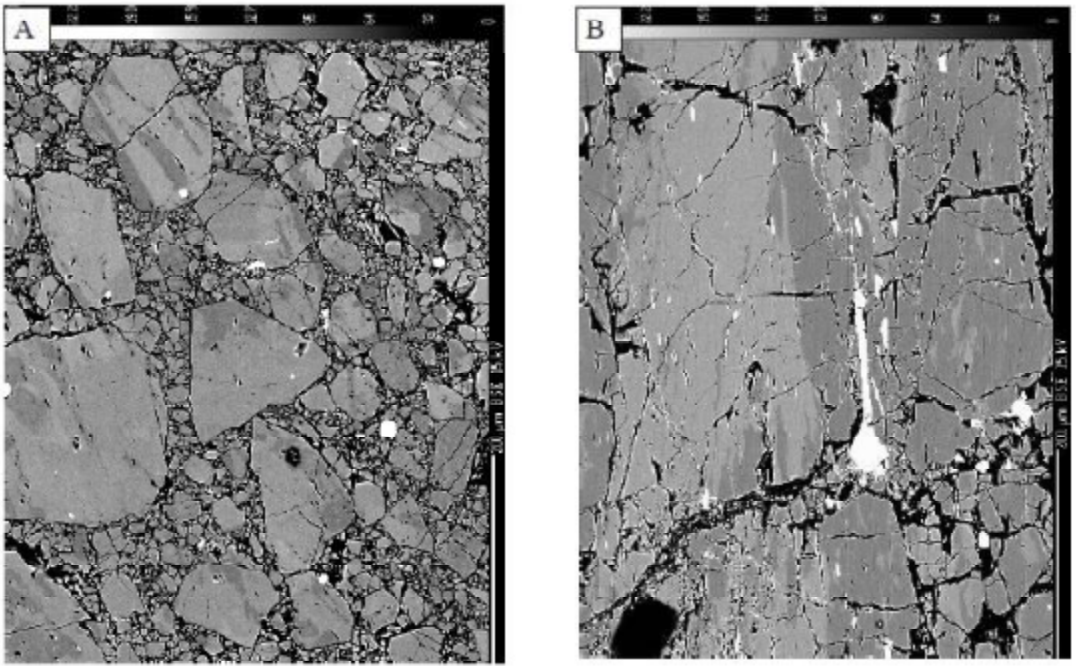

Figure 1: Back-scattered electron images showing: (A) coarse apatite grains in a brecciated matrix. The apatite grains show the patchy zonation. Note the extended pattern through the breccias. It shows the priority of dark-bright pattern to the brecciation. The white spots are monazite crystals; (B) The development of dark-bright pattern in the apatite, parallel to crystallographic c-axis. The elongated monazite inclusions have formed in the same direction. The monazite crystals in the brecciated areas are mostly different in shape.

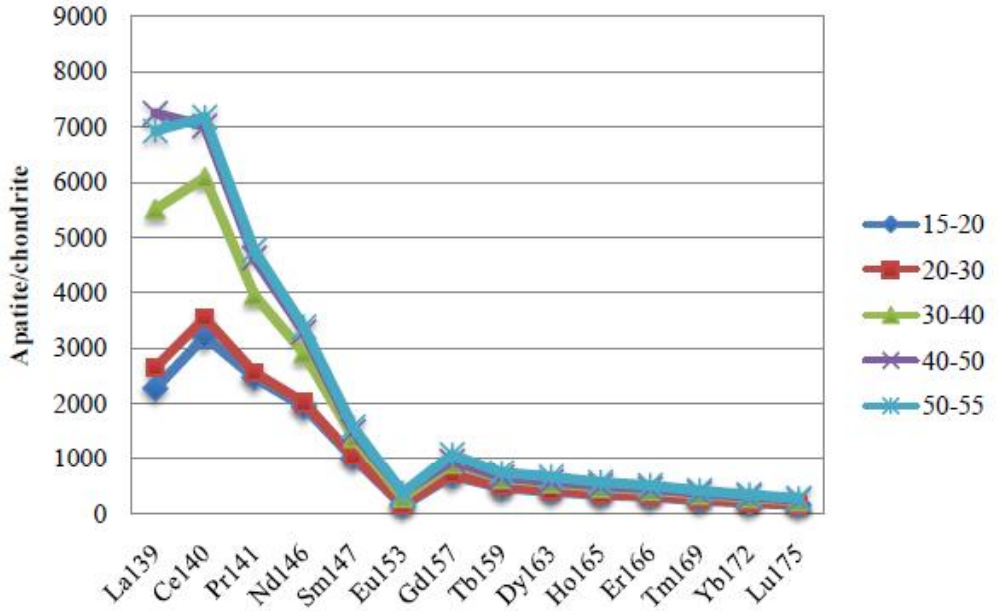

Figure 2: Chondrite normalized REE distribution patterns of dark and bright areas of apatite from Se-Chahun ore deposit, anomaly X. The pattern shows negative anomalies in Eu and slight positive anomaly in Ce. Note the lower concentration of the dark areas (40-50, 50-55) in both diagrams.